THE ASTROPHYSICAL JOURNAL, 418:626–637, 1993 December 1

THE INFRARED TULLY-FISHER RELATION IN THE URSA MAJOR CLUSTER

R. F. PELETIER
Kapteyn Laboratorium, Postbus 800, 9700 AV Groningen, The Netherlands, and European Southern Observatory, Garching bei München, Germany

AND

S. P. WILLNER
Harvard-Smithsonian Center for Astrophysics, 60 Garden Street, Cambridge, MA 02138
Received 1993 February 26; accepted 1993 June 7

ABSTRACT

We present new magnitudes derived from 1.65 μm images for 23 galaxies in the Ursa Major cluster. Magnitudes now exist for all but one spiral meeting our criteria for cluster membership and having H I velocity width greater than 187 km s^{-1} and inclination greater than 45°. These spirals fit a Tully-Fisher relation with dispersion in intrinsic magnitudes (after known observational uncertainties and the effect of cluster depth are removed) of 0.36 and a slope of 10.2 ± 0.6. The magnitude dispersion is smaller than found in the Virgo cluster but still significantly larger than claimed by some authors. We find a hint that the Tully-Fisher relation may turn over at the bright end. Adding the central surface brightness of the disk as a third parameter flattens the slope of the Tully-Fisher relation and may give a distance estimate with slightly less dispersion, but the significance of the decrease must be tested on an independent sample.

Subject headings: galaxies: clusters: individual (Ursa Major) — galaxies: photometry — infrared: galaxies

1. INTRODUCTION

The Tully-Fisher relation (Tully & Fisher 1977) is one of the most useful ways to measure distances to spiral galaxies (e.g., Jacoby et al. 1992). However, the amount of scatter in the Tully-Fisher relation is still a key issue, one of importance not only for estimating the distance uncertainties but also because the amount of scatter is crucial in estimating the bias in the distances themselves (Teerikorpi 1984, 1987; Bottinelli et al. 1987). Several authors have found remarkably small dispersions (e.g., Freedman 1990, review by Jacoby et al. 1992), but Fouqué et al. (1990) and Peletier & Willner (1991, hereafter Paper I) have found intrinsic dispersions among Virgo cluster spirals near 0.5 magnitudes in the blue and 0.4 magnitudes in the infrared.

The natural question is whether the large dispersions are a property of just the Virgo cluster or are inherent in the Tully-Fisher relation itself. An ideal test case is the Ursa Major cluster. It lies at nearly the same redshift as Virgo, has plenty of spiral galaxies, and earlier studies (Pierce & Tully 1988, hereafter PT) have indicated a smaller Tully-Fisher dispersion than in Virgo.

This paper presents magnitudes derived from infrared images for a nearly complete sample of Ursa Major spirals. The primary aim is to investigate the dispersion, but we also examine how best to derive magnitudes and inclinations for Tully-Fisher purposes. Sample selection is given considerable attention.

2. SAMPLE SELECTION

Selection of the sample to be studied is crucial both to avoid biases in the magnitudes, which could lead to bias in derived distances (Teerikorpi 1984, 1987; Kraan-Korteweg, Cameron, & Tammann 1988; Bottinelli et al. 1988), and to calculate the correct dispersion in the derived magnitudes (Paper I). An ideal sample would be selected without any reference whatever to galaxy magnitudes. Although the ideal is impossible, for such nearby clusters as Ursa Major a close approximation to the ideal can be achieved.

There are two methods commonly used to define cluster membership. The first is based on a nearest-neighbor analysis (e.g., Huchra & Geller 1982), while the second is simply to establish position and velocity limits. In the nearest-neighbor or "tree" analysis, a list of galaxies with positions, velocities, and magnitudes is somehow sorted according to the presumed "closeness" of the various galaxies. A density threshold is then established, and any selection of the list having density above the threshold is taken to be a group. This method assumes no a priori knowledge of cluster locations, but practical implementations (e.g., Tully 1987) often have an explicit dependence on galaxy magnitudes.

The second method is necessarily somewhat empirical. The position limits are usually expressed as a cluster center and radius, and minimum and maximum velocity limits are established. The advantage of this method is that there is no explicit dependence on galaxy magnitudes, though a dependence could arise if the original list is seriously incomplete at fainter magnitudes. Incompleteness is not a problem for this study, however, because catalogs contain galaxies fainter than 15th magnitude (though they are not complete at this limit, of course) while most of the spirals in the Ursa Major cluster are brighter than 12th in *B*.

For this study, we examined data compiled for the CfA Redshift Survey (Huchra et al. 1983, and unpublished). An initial examination in right ascension–declination–redshift space found distinct groupings at $V_h < 400$ km s^{-1}, $625 < V_h < 825$ km s^{-1}, $825 < V_h < 1025$ km s^{-1}, and $1100 < V_h < 1300$ km s^{-1}. The last group seems to be separated from the others in position, while the first three are separated mainly in velocity. The position centroid of those galaxies in the range $600 < V_h < 1050$ km s^{-1} is approximately 11^h54^m, 48°53′, which we have adopted as the cluster center.[1] The surface density of

[1] Compare with 11^h54^m, +49°30′ found by Biviano et al. (1990). PT used the same center coordinates as Biviano et al. along with a cluster radius of 7°.5 and effective velocity limits $628 < V_h < 1138$ km s^{-1}.

TABLE 1

BASIC DATA FOR SELECTED URSA MAJOR GALAXIES

Galaxy (1)	V_h (2)	d_c (3)	log (a/b) (4)	Type (5)	ΔV_{20} (6)	Uncertainty (7)	log ΔV^c_{20} (8)
NGC 3718.....	987	5.74	0.31	1	470	±3	2.726
NGC 3726.....	861	4.27	0.16	5	284	±4	2.589
NGC 3729.....	1096	5.66	0.17	1	214	±21	2.459
NGC 3769.....	724	3.23	0.50	3	272	±9	2.452
NGC 3877.....	903	2.09	0.63	5	368	±7	2.572
NGC 3893.....	977	1.32	0.21	5	302	±4	2.578
NGC 3917.....	975	3.34	0.61	6	293	±5	2.475
NGC 3949.....	786	0.89	0.24	4	276	±7	2.522
NGC 3953.....	1037	3.76	0.30	4	425	±7	2.687
NGC 3972[a].....	831	6.72	0.56	4	263	±8	2.433
NGC 3985.....	946	0.27	0.19	9	165	±11	2.327
NGC 3992[a].....	1051	4.77	0.21	4	475	±3	2.774
NGC 4010.....	905	1.39	0.73	7	269	±7	2.432
NGC 4013.....	835	4.67	0.71	3	407	±8	2.613
NGC 4085.....	750	2.24	0.55	5	292	±7	2.478
NGC 4088.....	752	2.41	0.41	4	363	±6	2.590
NGC 4096.....	559	1.96	0.57	5	325	±4	2.523
NGC 4100.....	1080	1.83	0.48	4	411	±7	2.633
NGC 4102.....	862	4.36	0.24	3	315	±8	2.580
NGC 4142.....	1141	4.91	0.27	7	187	±8	2.339
NGC 4157[a].....	771	2.98	0.70	3	413	±7	2.620
NGC 4183[a].....	934	5.76	0.83	6	249	±5	2.396
NGC 4217.....	1032	3.62	0.53	3	431	±6	2.650
NGC 4218[b].....	725	3.24	0.22	1	160	±8	2.296
NGC 4389.....	717	5.84	0.29	4	188	±5	2.337
UGC 6667.....	971	3.72	0.89	6	189	±8	2.276
UGC 6917[c].....	909	1.82	0.24	9	195	±7	2.371
UGC 6923[a].....	1065	4.56	0.38	10	173	±4	2.274
UGC 6983.....	1068	4.12	0.16	6	194	±5	2.424

NOTES.—(Col. [1]) Galaxy name; (col. [2]) heliocentric velocity from CfA redshift survey (Huchra et al. 1983, and private communication); (col. [3]) distance from center of UMa cluster; (col. [4]) log (axis ratio), from RC3; (col. [5]) galaxy type, from RC3; (col. [6]) H I width at 20% of the peak (from RC3); (col. [7]) uncertainty in col. (6); (col. [8]) logarithm of inclination-corrected velocity width.

[a] No images obtained; magnitudes from A82.

[b] Not observed.

[c] Bright foreground star; magnitudes could not be derived.

galaxies falls off beyond 7° from this position, so we have adopted this as the cluster radius even though there are undoubtedly cluster galaxies beyond this radius. Finally, we have slightly extended the velocity limits to $550 < V_h < 1150$ km s^{-1} in order to make our definition correspond more closely to previous work. All galaxies meeting these requirements are listed in either Table 1 or 2.[2] There is no explicit magnitude dependence in selecting this sample, or indeed any requirement that magnitudes be known, but galaxies must have been cataloged and had redshifts measured. This will introduce some incompleteness, but this probably becomes serious only below magnitude 14.

From the initial list, we have excluded 15 galaxies that are not spirals (keeping only galaxies with $T > 0$ according to the RC3—de Vaucouleurs et al. 1991). Only reasonably edge-on galaxies can give useful velocity widths, so we have excluded 13 galaxies with axis ratio less than 1.40 corresponding to inclination less than 45° (Paper I). Finally, we have excluded 17 galaxies that lack H I observations or have inclination-corrected velocity widths $\Delta V^c_{20} < 187.5$ km s^{-1}, an arbitrary limit reflecting the completeness of our photometric observations. Many of the excluded galaxies are faint, but it is possible that better H I observations would allow some of them to be used for Tully-Fisher purposes. Table 2 lists all the excluded galaxies.

The remaining cluster sample contains 29 galaxies listed in Table 1. In practice, an almost identical sample would have been obtained from nearest-neighbor analysis simply by adopting group "12-1" from Tully (1987).[3] This group has 57 members, and other authors of nearest-neighbor analyses (Geller & Huchra 1983; Huchra & Geller 1982; Turner & Gott 1976) consider it a subgroup of their somewhat larger groups. The difference seems to arise because the latter authors are interested in larger structures and accordingly have set their density thresholds lower. For this study, we need to be sure all the galaxies are at the same distance, so the most restrictive definition is appropriate.

Two of the galaxies in Table 1 lack infrared magnitudes. UGC 6917 has a bright star superposed on the galaxy, rendering the current observations useless, and we failed to observe NGC 4218. A total of 27 galaxies are thus available for analysis.

[2] All galaxies in Tables 1 and 2 except two are cataloged galaxies for which positions and other data can be found in the NASA Extragalactic Database (NED). 115400+4836 (KDG 310A) is a companion south preceding NGC 3985 (KDG 310B). We do not know of published data on 115640+5059. These three galaxies are among those excluded from our Tully-Fisher sample and were not observed.

[3] The only differences affecting Table 1 are that Tully (1988, hereafter NBG) assigns NGC 3985 and 4096 to group 14-4. The former galaxy has an incorrect heliocentric velocity in the NBG, and it seems it would have been considered a member of 12-1 if the correct velocity had been used. The latter is on the outskirts of both groups and might belong to either.

TABLE 2A

REJECTED URSA MAJOR GALAXIES: GALAXIES WITH TYPE ≤0 OR PECULIAR

Galaxy (1)	V_h (2)	d_c (3)	log (a/b) (4)	Type (5)
NGC 3870.....	750	2.34	0.09	−2
NGC 3896.....	906	1.27	0.15	0
NGC 3931.....	928	3.50	0.09	−3
NGC 3990.....	705	6.85	0.24	0
NGC 3998.....	1028	6.85	0.08	0
NGC 4026.....	944	2.40	0.61	−2
NGC 4111.....	806	5.85	0.67	−1
NGC 4117.....	958	5.85	0.31	−2
NGC 4138.....	835	5.45	0.18	−1
NGC 4143.....	966	6.52	0.20	−2
NGC 4220.....	954	3.36	0.45	−1
NGC 4346.....	762	4.86	0.42	−2
NGC 4460.....	558	6.82	0.53	−1
UGC 6805.....	1033	6.66	0.12	E?
UGC 6818.....	803	2.98	0.33	SB?

TABLE 2B

REJECTED URSA MAJOR GALAXIES: GALAXIES WITH INCLINATION LESS THAN 45°

Galaxy (1)	V_h (2)	d_c (3)	log (a/b) (4)	Type (5)
NGC 3906.....	962	1.16	0.05	7
NGC 3913.....	953	6.80	0.01	7
NGC 3928.....	974	0.79	0.00	3
NGC 3924.....	1003	1.55	0.04	9
NGC 3938.....	812	4.53	0.04	5
NGC 4051.....	710	4.24	0.13	4
UGC 6628.....	849	3.93	0.00	9
UGC 6713.....	896	2.03	0.14	9
UGC 6922.....	892	2.21	0.09	S?
UGC 6956.....	916	2.33	0.03	9
UGC 6962.....	809	5.88	0.09	6

TABLE 2C

REJECTED URSA MAJOR GALAXIES: GALAXIES WITHOUT H I DATA, WITHOUT H I, OR WITH $\Delta V^c_{20} < 187.5$ km s^{-1}

Galaxy (1)	V_h (2)	d_c (3)	log (a/b) (4)	Type (5)	ΔV_{20} (6)	Uncertainty (7)	log ΔV^c_{20} (8)
NGC 3769A	791	3.23	0.38	9			
NGC 3782	740	3.63	0.19	6	132	7	2.230
UGC 6399	779	5.72	0.55	9	166	16	2.233
UGC 6446	646	6.78	0.19	7	143	6	2.272
UGC 6773	925	1.83	0.29	10			
UGC 6840	1016	3.57	0.50	9	149	6	2.190
UGC 6894	767	6.05	0.78	6	155	9	2.191
UGC 6930	776	0.68	0.20	7	133	8	2.228
UGC 6969	1113	4.83	0.50	10	157	10	2.213
UGC 6973	704	5.90	0.35	2			
UGC 7089	778	5.73	0.69	8	153	9	2.190
UGC 7176	859	2.84	0.49	10	111	9	2.064
UGC 7218	791	4.43	0.29	10	107	8	2.090
UGC 7301	712	4.31	0.88	7	144	9	2.158
Mark 1460.....	768	1.02					
115400+4836	886	0.28					
115640+5059	963	2.14					

NOTES, TABLES 2A–2C.—(Col. [1]) galaxy name; (col. [2]) heliocentric velocity from CfA redshift survey (Huchra et al. 1983, and private communication); (col. [3]) distance from center of UMa cluster; (col. [4]) logarithm of axis ratio from RC3; (col. [5]) galaxy type from RC3; (col. [6]) H I width at 20% of the peak (from RC3); (col. [7]) uncertainty in col. (6); (col. [8]) logarithm of inclination-corrected velocity width.

3. OBSERVATIONS

All of the observations were made with the 1.2 m telescope at Mount Hopkins and the Smithsonian Observatory Near-Infrared Camera (SONIC). This camera is the same one used with the 0.6 m telescope for Paper I. Twenty galaxies were observed in 1991 and four in 1992 through a standard (Barr Associates) 1.65 μm ("H") bandpass filter. Observations in 1991 January through March used a two-lens reimaging optical system giving a scale of 1".641 per pixel, while those in 1992 March used a three-lens optical system giving 1".757 per pixel. Sky frames were observed along with each galaxy, separated from object frames by more than 3 arcmin depending on the galaxy size.

Data calibration began by removing dark current and star images from sky frames and averaging sky frames to create a flat field. Each object frame, including those for standard stars, was divided by a flat-field frame. The observations of standard stars showed a variation of up to 30% peak-to-peak in 1991 and 20% in 1992 depending on where the standard star fell on the object frame. The variation was repeatable and mostly in the east-west direction. We attribute it to the incomplete long-wavelength blocking of the 1.65 μm bandpass filter; the sky frames thus contain a component at ~ 5 μm, while the much bluer stars contain no such component. Since the quantum efficiency of the detector is a function of wavelength as well as position, the incomplete blocking leads to the sky flats being inaccurate when applied to stars. The change from 1991 to 1992 is attributed to addition of a glass blocker, but obviously a thicker blocker is needed (and has since been added).

Fortunately, it is easy to calibrate the responsivity variation since nearly all standard stars were observed at many positions on the detector array. A linear function of pixel x-y coordinates was derived for each night, though in practice there was no

TABLE 3

PHOTOMETRIC RESULTS

Galaxy (1)	D_0 (2)	$H^c_{-0.5}$ (3)	± (4)	$H^e_{-0.5}$ (5)	± (6)	H_{19} (7)	± (8)	$H^{0.7}_{20}$ (9)	± (10)
NGC 3718	476.6	8.29	0.19	8.43	0.13	8.62	0.08	8.57	0.09
NGC 3726	353.3	8.85	0.30	8.98	0.22	9.32	0.16	9.21	0.18
NGC 3729	177.1	9.53	0.10	9.77	0.05	9.41	0.06	9.40	0.06
NGC 3769	157.8	9.94	0.09	10.42	0.05	10.10	0.06	10.16	0.06
NGC 3782	97.3	11.69	0.05						
NGC 3877	250.1	8.67	0.06	9.28	0.05	8.66	0.05	8.82	0.05
NGC 3893	244.4	8.72	0.08	8.92	0.06	8.79	0.07	8.79	0.07
NGC 3917	233.4	9.93	0.09	10.72	0.05	10.61	0.05	10.25	0.05
NGC 3949	165.3	9.37	0.05	9.63	0.05	9.29	0.05	9.30	0.05
NGC 3953	361.5	7.91	0.09	8.17	0.06	7.99	0.07	8.02	0.07
NGC 3972	194.2	10.46	0.05						
NGC 3985	70.5	11.35	0.05	11.56	0.05	11.15	0.05	10.94	0.05
NGC 3992	424.8	7.95	0.05						
NGC 4010	185.4	10.44	0.10	11.05	0.05	10.97	0.05	10.71	0.05
NGC 4013	233.4	8.53	0.11	8.90	0.05	8.26	0.08	8.20	0.08
NGC 4085	137.5	9.99	0.05	10.47	0.05	10.07	0.05	10.15	0.05
NGC 4088	293.9	8.33	0.13	8.81	0.08	8.27	0.12	8.41	0.10
NGC 4096	307.7	8.84	0.08	9.36	0.05	9.10	0.05	9.08	0.05
NGC 4100	261.9	8.83	0.10	9.36	0.06	8.88	0.07	9.06	0.07
NGC 4102	177.1	8.42	0.05	8.56	0.05	8.31	0.05	8.39	0.05
NGC 4142	128.3	12.10	0.07	12.47	0.05	16.07	0.08	13.16	0.05
NGC 4157	307.7	8.32	0.05						
NGC 4183	212.9	10.64	0.05						
NGC 4217	268.0	8.59	0.05	8.99	0.05	8.65	0.05	8.65	0.05
NGC 4389	150.7	10.45	0.05	10.69	0.05	10.89	0.05	10.51	0.05
UGC 6667	143.9	12.14	0.07	13.13	0.05	14.11	0.05	13.22	0.05
UGC 6923	104.3	12.04	0.05						
UGC 6983	222.9	11.55	0.20	11.77	0.05	14.99	0.06	13.45	0.07
Extra galaxy, not in sample:									
UGC 6894	62.8	13.71	0.08	14.74	0.06	<16.00	0.10	14.76	0.06

NOTES.—(Col. [1]) Galaxy name; (col. [2]) isophotal diameter D_0, corrected for Galactic extinction and inclination; (col. [3]) circular magnitude inside $0.316D_0$ (derived from A82 if other magnitudes are missing); (col. [4]) uncertainty in col. (3); (col. [5]) elliptical magnitude inside $0.316D_0$; (col. [6]) uncertainty in col. (5); (col. [7]) elliptical magnitude inside $D_{19,i}$; (col. [8]) uncertainty in col. (7); (col. [9]) elliptical magnitude inside $0.7D_{20,i}$; (col. [10]) uncertainty in col. (9).

significant variation from night to night. A normalized sky frame was subtracted from each object frame, then the result was multiplied by the correction frame. This procedure should work well because the standard stars are nearly the same color as the galaxies. Finally, the various object frames were averaged and mosaicked together.

Typical final galaxy frames consist of images taken at 2 to 5 positions, mosaicked with usually the galaxy nucleus as a reference point or sometimes a bright star or an H II region. Figure 1 (Plate 11) shows gray-scale images of a bright, intermediate, and faint galaxy in the sample. The dark current fluctuations mentioned in Paper I had been cured, so the present observations reach typical 1 σ noise levels of $20.7H$ mag arcsec^{-2} for bright galaxies and $21.2H$ mag arcsec^{-1} for the faintest galaxies. These values imply that our photometry is limited by the accuracy to which the sky background can be determined on the frames. This in turn is limited by the small field size and by the extent to which the images could be corrected for the unblocked long-wavelength light. By looking at the dispersion in the sky values measured at various corners on the frames, these uncertainties have been estimated and are given in Table 3 for the various types of magnitudes.

On 9 out of 11 nights the weather conditions were photometric. On these nights the photometric zero points were calibrated using standard stars from Elias et al. (1982). Typically on each night five to six red and blue standard stars were observed at various positions on the frame. Internal consistency was better than 0.02 mag. No color term was applied to the calibration. On the other two nights the zero points were calibrated using aperture photometry from Aaronson et al. (1982, hereafter A82).

Given the fact the galaxy frames were well behaved and of a much better quality than those for Virgo in Paper I, accurate surface brightness profiles could be determined. Radial profiles of surface brightness, ellipticity, and position angle were determined using GALPHOT, the two-dimensional ellipse-fitting package written by M. Franx (Jørgensen, Franx, & Kjærgaard 1992). Not only did we determine from them the axis ratio and the position angle in the outer parts, to get the infrared inclinations, but also a bulge-disk decomposition was performed. Analysis of the photometric profiles will be given in a later paper, but we will deal with whether bulge-disk decomposition can improve the Tully-Fisher relation in § 4.

4. INGREDIENTS FOR THE TULLY-FISHER RELATION

4.1. *Magnitudes in Circular Beams*

Since infrared arrays have only recently become available, people up to now have used magnitudes in circular beams for the infrared Tully-Fisher relation. Aaronson and coworkers (Aaronson, Huchra, & Mould 1979, hereafter AHM; Aaronson, Mould, & Huchra 1980, hereafter AMH; Aaronson et al. 1986; Bothun et al. 1985) have used the magnitude inside circular beams with diameters of $0.316D_1$, in which D_1 is the isophotal diameter at $B = 25$ mag arcsec^{-2} corrected for Galactic extinction and inclination (see AMH). To test the reliability of our photometry we have determined the magnitudes inside $0.316D_1$ for the galaxies that overlap between A82 and this paper. The comparison is shown in Figure 2. The mean difference, 0.02 mag, and the dispersion, 0.03 mag, are well within the uncertainties of our data, even for the faintest galaxies. It shows that, if anything, our photometric uncertainties have been overestimated.

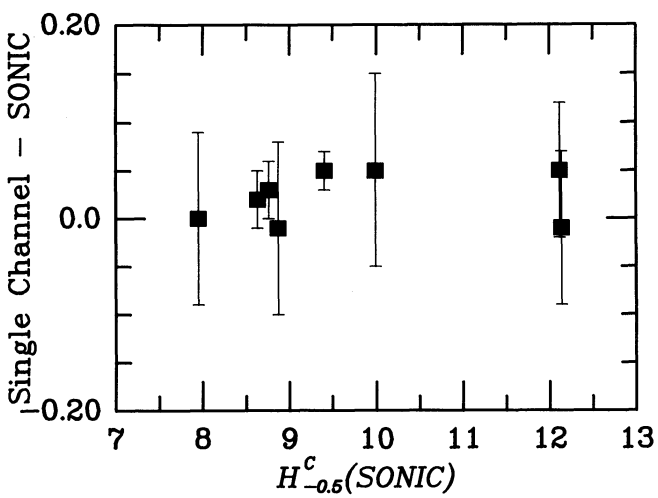

FIG. 2.—Comparison between SONIC magnitudes and magnitudes from single-detector aperture photometry (A82). For this figure only, SONIC magnitudes are measured in circular apertures of diameter A such that $\log(A/D_1) = -0.5$.

1993ApJ...418..626P

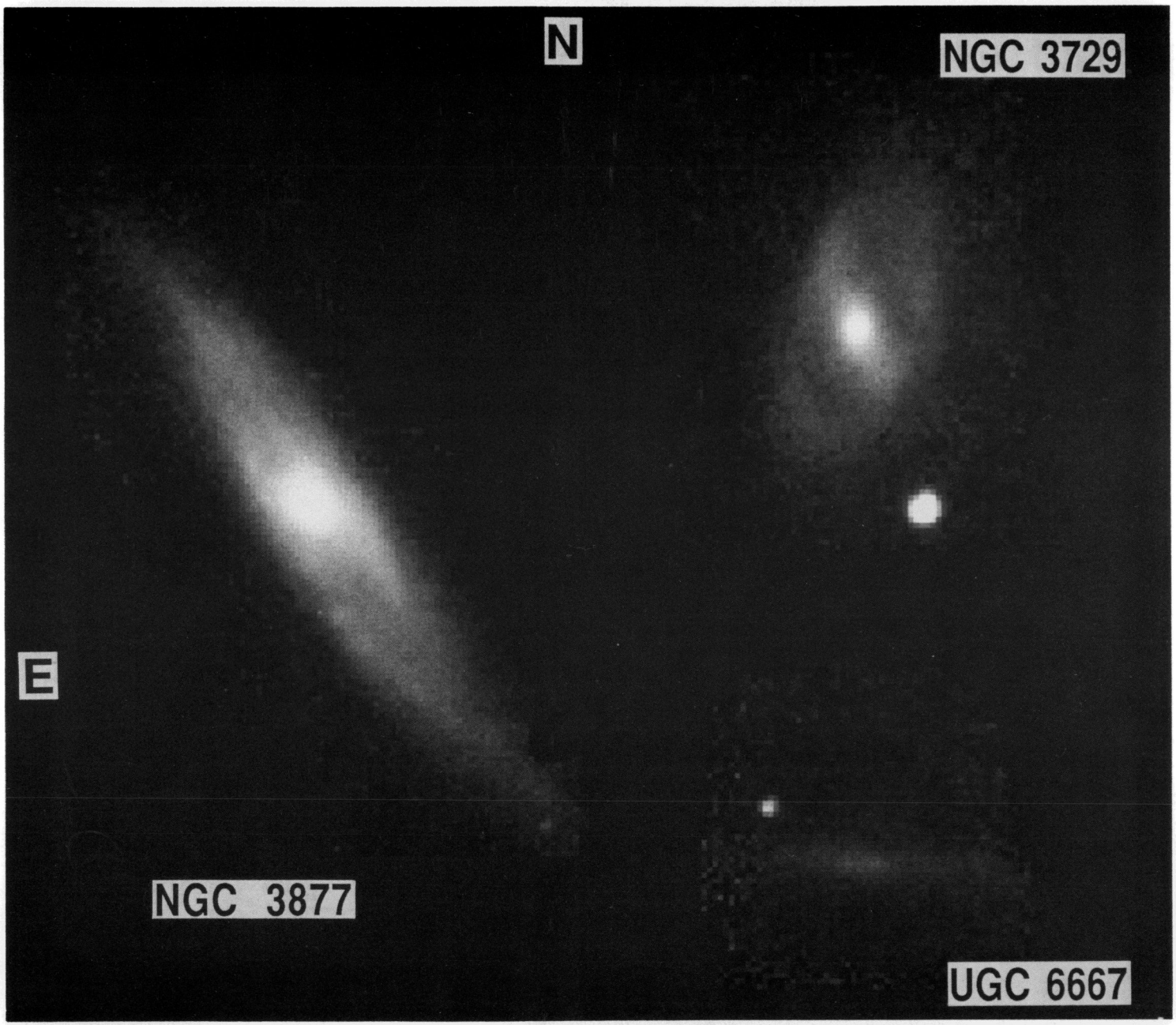

FIG. 1.—Images of three galaxies in the sample, NGC 3877, one of our largest galaxies, NGC 3729, an intermediate size galaxy, and UGC 6667, one of our smallest galaxies. The three are shown on the same angular and intensity scales, and the lower central surface brightness of the fainter galaxies can be seen.

PELETIER & WILLNER (see 418, 629)

Table 3 (col. [3]) lists circular magnitudes ($H^c_{-0.5}$) for sample galaxies in diameters of $0.316D_0$. Here D_0 is the blue isophotal diameter again at 25 B mag arcsec^{-2} but now corrected for Galactic extinction and inclination following the recipe of the RC2 (de Vaucouleurs et al. 1976), analogous to Paper I. The diameter D_0 is similar to D_1 and in fact is just $1.05D_1$ for our galaxies. The inclination correction is meant to make sure that the same fraction of the infrared light is measured for each galaxy and corrects for the fact that the ratio of effective to isophotal radii decreases with inclination for transparent galaxies. The inclination correction was not applied to blue magnitudes in the RC3, since its authors were convinced that spiral galaxy disks have surface brightness independent of inclination in B. For H magnitudes, however, the correction must be applied, since in this band spiral galaxies are more or less transparent (Peletier & Willner 1992).[4] For those galaxies in Ursa Major that are included in A82 for which we do not have infrared images, the circular magnitude inside $0.316D_0$ was calculated from the value inside $0.316D_1$ using the average difference for the galaxies in common (-0.03 mag). These galaxies can be identified by the absence of additional magnitudes in Table 3.

4.2. *Magnitudes in Elliptical Beams*

An advantage of imaging is flexibility in choosing the kind of magnitudes to use. To investigate whether the scatter in the Tully-Fisher law might decrease using different magnitudes we have determined magnitudes in elliptical beams within the optically determined $0.316D_0$ as well as elliptical magnitudes in diameters determined from infrared isophotes. For the latter, no information from the optical is needed. Defining $D_{\mu,i}$ as the major axis diameter of the isophote at surface brightness μ, corrected for inclination using the recipe of the RC2 with infrared axis ratios, we have calculated for each galaxy the magnitudes inside $D_{19,i}$ and $0.7D_{20,i}$, to be called H_{19} and $H^{0.7}_{20}$. We used $0.7D_{20,i}$ instead of $D_{20,i}$ because of the limited field of some images. These magnitudes have also been tabulated in Table 3.

4.3. *Total Magnitudes*

Even though we never cover the entire galaxy, it is possible, with some assumptions, to derive a good approximation for the total magnitudes. The reason is that the spiral galaxies of Ursa Major can be fit rather well by a central bulge and an exponential disk. Total magnitudes can be found simply by extrapolating the disk outward. Schommer et al. (1993) have examined this method for I-band images and emphasized its difficulties: because galaxy surface brightness profiles show bends and wiggles, the uncertainty of any extrapolation is increased and difficult to estimate. There is little doubt that deeper images would be preferable, but the uncertainties in the total magnitudes derived this way are still less important than the uncertainties in velocity widths and inclinations.

We have performed the bulge-disk decompositions using the method described by Kent (1986). This method uses the surface brightness profiles on the major and minor axes and assumes that bulge and disk both have a constant axis ratio with the bulge being rounder than the disk. After the decomposition, we fit an exponential to the surface brightness profile of the disk, excluding the inner areas in which the bulge dominates. The luminosity of the disk is calculated analytically,[5] and the bulge luminosity is determined on the frame of each galaxy after having subtracted the model disk. Since for almost all galaxies the bulge is much smaller than the disk, the decomposition is unambiguous, and the uncertainties in the total magnitudes should be comparable to those in the circular magnitudes. Table 4 gives the ellipticities of bulge and disk, total magnitudes, bulge to disk ratios, scale lengths, central disk surface brightness, and total magnitudes of the disk.

TABLE 4

BULGE-DISK DECOMPOSITION

Galaxy (1)	ϵ_B (2)	ϵ_D (3)	ϕ_D (4)	H_T (5)	B/D (6)	h_D (7)	$H(0)$ (8)	H_D (9)
NGC 3718	0.07	0.17	112	8.05	0.41	26.8	17.41	8.43
NGC 3726	0.30	0.47	112	8.22	0.05	37.6	17.50	8.27
NGC 3729	0.18	0.36	84	8.64	0.03	21.9	16.93	8.67
NGC 3769	0.20	0.65	63	9.45	0.10	17.5	16.66	9.55
NGC 3877	0.21	0.77	123	8.26	0.06	28.9	16.06	8.32
NGC 3893	0.15	0.38	42	8.24	0.46	26.5	17.29	8.65
NGC 3917	0.30	0.73	167	8.67	0.02	52.6	17.92	8.69
NGC 3949	0.37	0.44	32	8.73	0.26	20.1	16.90	8.98
NGC 3953	0.23	0.47	102	7.43	0.11	34.6	16.59	7.54
NGC 3985	0.33	0.34	10	10.33	0.11	11.1	17.25	10.44
NGC 4010	0.50	0.84	155	9.50	0.03	35.7	17.35	9.54
NGC 4013	0.15	0.84	154	7.74	0.09	34.1	15.54	7.83
NGC 4085	0.15	0.67	165	9.11	0.06	20.5	16.56	9.17
NGC 4088	0.30	0.61	143	7.58	0.03	39.3	16.61	7.62
NGC 4096	0.25	0.72	108	7.99	0.08	50.5	17.25	8.07
NGC 4100	0.25	0.67	75	8.15	0.05	36.1	16.82	8.20
NGC 4102	0.11	0.27	131	7.96	0.56	18.9	16.52	8.44
NGC 4142		0.33	89	11.23	0.00	16.0	18.85	11.23
NGC 4217	0.42	0.85	139	7.84	0.03	47.7	16.24	7.87
NGC 4389	0.70	0.79	14	9.27	0.07	39.4	17.67	9.35
UGC 6667	0.00	0.84	177	11.00	0.03	32.7	18.65	11.03
UGC 6983		0.30	180	11.00	0.01	17.0	18.43	11.01
Extra galaxy, not in sample:								
UGC 6894		0.86	2	12.21	0.00	23.0	18.91	12.21

NOTES.—(col. [1]) Galaxy name; (col. [2]) ellipticity of bulge; (col. [3]) ellipticity of disk; (col. [4]) position angle of galaxy disk (north through east); (col. [5]) total H magnitude; (col. [6]) bulge to disk ratio (in luminosity); (col. [7]) H scale length of disk; (col. [8]) central disk surface brightness; (col. [9]) total magnitude of disk.

4.4. *Which Magnitudes Are Best?*

Each type of magnitude discussed above has been fit to a linear Tully-Fisher relation, taking into account uncertainties in both magnitudes and velocity widths. Since the latter are so much larger than the former, the procedure is almost equivalent to using magnitude as the independent variable, i.e., to the "inverse Tully-Fisher relation" discussed by Fouqué et al. (1990). The results are shown in Figure 3 and Table 5, where column (6) gives the reduced chi-square of the fit and column (7) shows the additional magnitude uncertainty that must be added (in quadrature) to make $\chi^2_{\rm red} = 1$.

The smallest scatter is found for circular magnitudes, in agreement with Paper I. The scatter increases only slightly for elliptical magnitudes but is much greater with infrared isophotal magnitudes. These have the advantage that they can be

[4] We make no representation that this is the best possible method of determining a diameter, but the prescription is well defined, the method is commonly used, and no other method has been shown to be better (§ 4.4).

[5] For an exponential disk with major axis profile $H(r) = H(0) \exp(-r/h)$ and major to minor axis ratio a/b, the integrated luminosity is $2\pi(b/a)h^2H(0)$.

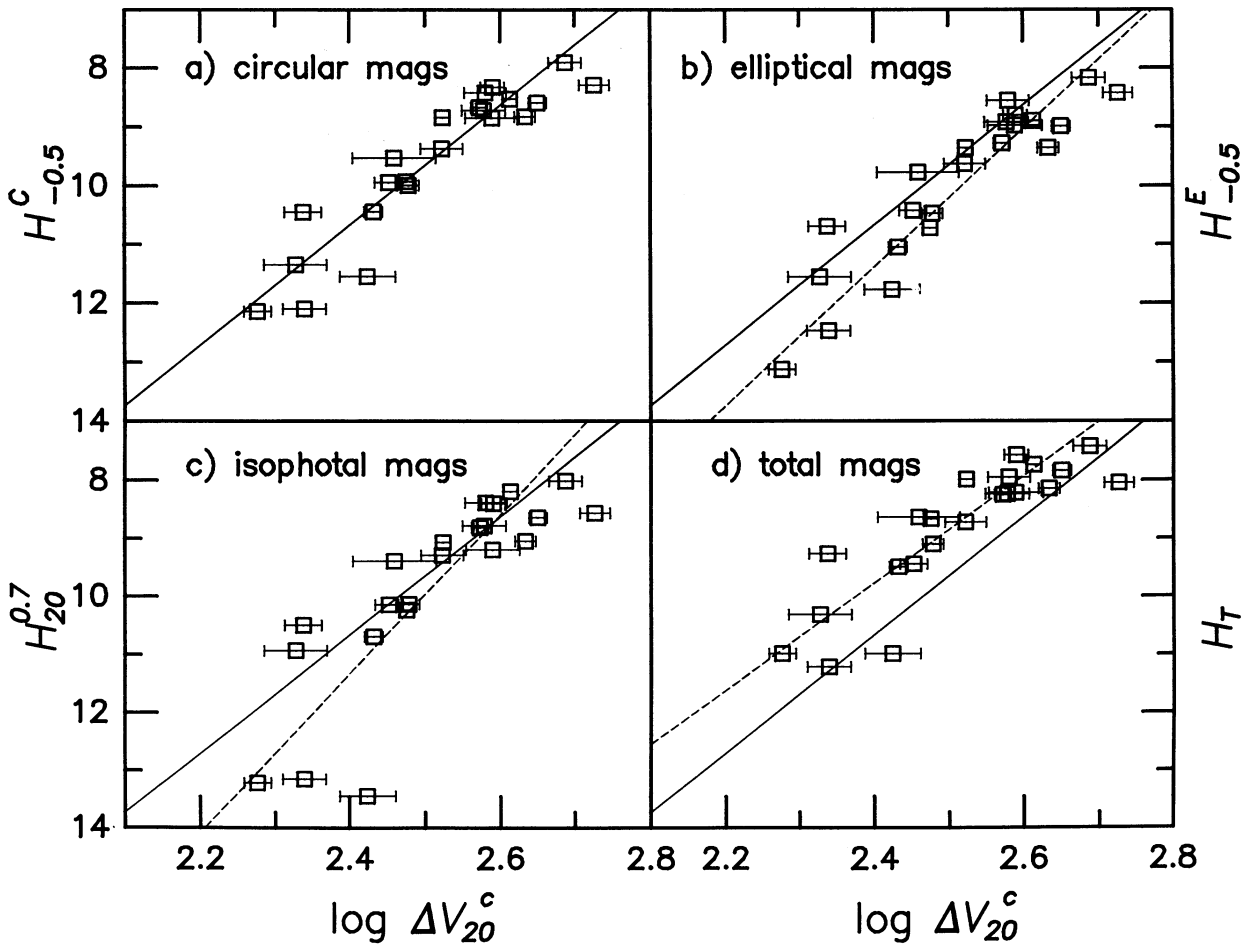

FIG. 3.—Tully-Fisher diagram with (*a*) circular, (*b*) elliptical, (*c*) isophotal, and (*d*) total magnitudes for the SONIC sample only. Error bars are shown for the velocity widths only. Except for a few galaxies (Table 3), the error bars on the magnitudes are about the size of the symbols. The solid lines show the Tully-Fisher relation fit to the baseline sample. Since the elliptical magnitudes are fainter, they tend to fall below this line. The dashed lines show the best fits for the elliptical, isophotal, and total magnitudes.

obtained without needing optical images, but they do not give very satisfactory results. The problem is that both bulge-to-disk ratios and disk surface brightnesses decrease as a function of velocity width, which means that some galaxies barely reach the isophote of 19 mag arcsec^{-2}. The Tully-Fisher relation with these magnitudes thus displays a large amount of curvature, as shown in Figure 3, with especially the faintest galaxies seeming much too faint for their velocity widths. Optical isophotal magnitudes or infrared magnitudes within optically determined diameters work much better because of the much smaller scatter in the central surface brightness of disks in *B* as opposed to *H* (Freeman 1970; Peletier & Willner 1992).

With total disk magnitudes or total magnitudes the scatter is slightly higher than when using circular magnitudes. Although in most cases bulge-to-disk ratios are small and exclusion of a bulge does not affect significantly the residual from the Tully-Fisher relation, NGC 3718 is different. This galaxy deviates considerably if its bulge is excluded. At least for this galaxy, the Tully-Fisher relation does not purely involve the disk but rather the whole galaxy.

In what follows, we adopt the magnitudes in circular beams.

4.5. *Velocity Widths*

All velocity widths used are H I velocity widths from Bottinelli et al. (1990), a large compilation of the literature. Since uncertainties in the velocity widths are unimportant compared to uncertainties in inclination, and since the errors for Ursa Major are on the average 8 km s^{-1}, compared to 13.5 km s^{-1} in our Virgo sample (Paper I), we have made no further attempt to select the best individual observations.

The only question in velocity is whether it is important to correct them for nonrotational motions (Tully & Fouqué 1985). The correction affects only the faintest galaxies. Table 5 shows that replacing ΔV^c_{20} by corrected widths W_R (Tully & Fouqué 1985) does not improve the quality of the fit either for circular or for total magnitudes.

In what follows, we have used width ΔV^c_{20} corrected only for inclination and not for nonrotational motion.

4.6. *Inclinations*

Paper I found that the best way to determine galaxy inclinations is to use optical axis ratios in the outer parts. Inclinations determined in the infrared often suffer from central bars or strong spiral arms, because of the small field. However, infrared inclinations might turn out to be better than optical ones if the surface photometry is deep and the field large enough.

Even though the surface photometry for this paper goes approximately 2 mag deeper than in Paper I, the agreement between infrared and optical inclinations is no better. Figure 4 shows the difference between the inclinations. Here an intrinsic

TABLE 5

LEAST-SQUARE FIT RESULTS—INGREDIENTS OF THE TULLY-FISHER RELATION

Magnitude Type (1)	Nonrotational Correction (2)	Inclination Source (3)	Sample (4)	N_{gal} (5)	χ^2_{red} (6)	Δ(mag) (7)	Slope (8)	Intercept (9)
Changing Magnitude Type								
$H^c_{-0.5}$	no	RC3	SONIC	22	4.61	0.41	0.096	2.564
$H^e_{-0.5}$	no	RC3	SONIC	22	5.46	0.49	0.085	2.603
H_{19}	no	RC3	SONIC	22	11.31	1.35	0.055	2.568
$H_{20}^{9.7}$	no	RC3	SONIC	22	8.35	0.84	0.073	2.571
H_D	no	RC3	SONIC	22	7.55	0.54	0.110	2.493
H_T	no	RC3	SONIC	22	6.87	0.52	0.108	2.484
Changing Type of Velocity Width								
H_T	yes	RC3	SONIC	22	7.29	0.51	0.125	2.422
$H^c_{-0.5}$	no	RC3	Table 1	27	4.32	0.40	0.098	2.564
$H^c_{-0.5}$	yes	RC3	Table 1	27	4.64	0.39	0.112	2.515
Changing Inclinations								
$H^c_{-0.5}$	no	IR	SONIC	22	9.29	0.64	0.110	2.563
H_T	no	IR	SONIC	22	12.92	0.70	0.122	2.470

NOTES.—(col. [1]) Type of H-magnitude (Tables 3, 4); (col. [2]) correction for nonrotational motion (W_R); (col. [3]) source of inclinations; (col. [4]) sample (The "SONIC" sample consists of the galaxies in Table 1 excluding the five that lack images.); (col. [5]) number of galaxies in sample; (col. [6]) reduced χ^2 of fit; (col. [7]) additional uncertainty in the H-magnitudes necessary to bring χ^2 down to unity; (cols. [8] and [9]) best slope a and intercept b for $\log \Delta V = -a(H - 9.0) + b$.

axis ratio of 0.15 was assumed in the blue as well as the infrared (cf. Bottinelli et al. 1983) because several galaxies were inconsistent with the conventional value of 0.20 (e.g., AHM; Helou, Hoffman, & Salpeter 1984). The infrared inclinations confirm that some galaxies have intrinsic thickness smaller than $b/a = 0.20$ in this band as well. The comparison between infrared and blue inclinations here is qualitatively different from Paper I. Although the agreement for 16 out of 23 galaxies is better than 4 degrees, the others show very large differences in both directions. In most cases the difference is caused by a faint envelope visible on optical plates, but for NGC 4102 and NGC 4217 the differences are hard to explain this way.

Using infrared inclinations in the Tully-Fisher relation increases rather than decreases the scatter for all types of magnitude. Most of this is due to NGC 4389, which has a large residual to the Tully-Fisher relation. Since its infrared inclination is large, this will increase the residual and decrease at the same time the apparent uncertainty in ΔV^c, making the scatter much worse. However, even without NGC 4389 the scatter is larger when using infrared inclinations. For the subsample in common with PT, the scatter decreases if CCD inclinations are used. It might therefore be worthwhile to obtain CCD inclinations for the whole sample.

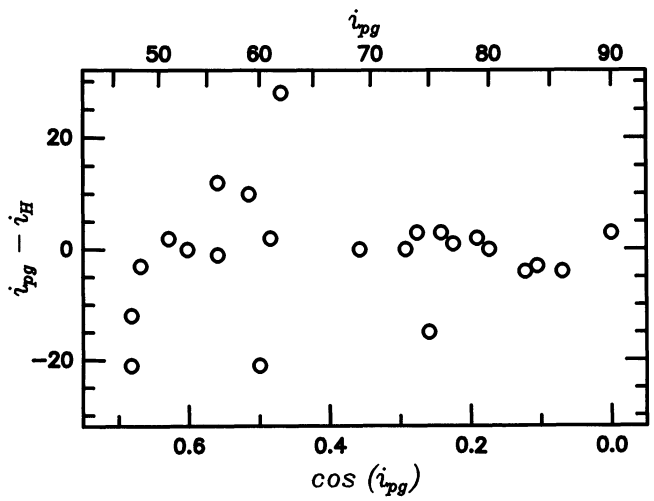

FIG. 4.—Comparison between inclinations derived from RC3 axis ratios (blue photographic measurements) and from infrared images. For many galaxies the agreement is very good, but for others the difference can exceed 10°.

PT obtained inclinations for many Ursa Major galaxies using CCD photometry. The average difference between the inclination derived by PT and from the RC3 is 1°.8 with a scatter (rms) of 4°.6. The situation here is similar to that in Virgo, for which we claimed (Paper I) that the uncertainty in the inclination of a typical galaxy is 5 degrees. Intrinsic uncertainties, like an axis ratio that varies with radius, spiral arms in the outer regions, and slightly triaxial shapes (Franx & de Zeeuw 1992) make it very difficult to see how this uncertainty can be reduced. Schommer et al. (1993) derived inclinations both photometrically (I-band) and from kinematic fits to the velocity field of the gas and thereby produced Tully-Fisher relations for two clusters with a *total* scatter of less than 0.30 mag. Kinematic inclinations or a combination of photometric and kinematic inclinations thus seem quite promising. However, the two methods give large ($>10°$) differences in inclination for some galaxies, and caution seems advisable until these differences can be understood.

4.7. *Type Dependence*

No dependence of the Tully-Fisher relation on galaxy type was found, in agreement with Paper I.

4.8. *More Parameters to Reduce the Scatter*

With the advantage of having images, we have investigated whether the residuals from the Tully-Fisher relation correlate with other galaxy parameters. Although for most parameters

TABLE 6

MULTIPLE PARAMETER FITS

Magnitude Type (1)	Sample (2)	N_{gal} (3)	Δ(mag) (2 par) (4)	Δ(mag) (3 par) (5)	Relation Derived (H =) (6)
$H^c_{-0.5}$	SONIC	22	0.41	0.35	$21.41 - 7.74 \log \Delta V^c + 0.44H(0)$
$H^c_{-0.5}$	Omit NGC 4389	21	0.37	0.32	$23.16 - 8.29 \log \Delta V^c + 0.43H(0)$
H_T	SONIC	22	0.52	0.45	$15.96 - 6.10 \log \Delta V^c + 0.48H(0)$
H_T	Omit NGC 4389	21	0.47	0.41	$18.11 - 6.77 \log \Delta V^c + 0.45H(0)$

NOTES.—(col. [1]) Type of H-magnitude; (col. [2]) sample; (col. [3]) number of galaxies in sample; (col. [4]) additional uncertainty in the H-magnitudes necessary to bring χ^2_{red} down to unity with fit based on magnitudes and velocity widths alone; (col. [5]) same as col. (4) but with $H(0)$ as a third parameter; (col. [6]) best-fitting plane.

the correlation is weak, the central disk surface brightness may have a useful effect. Table 6 gives the results of fitting a plane to the data in the space of magnitudes, velocity widths, and central surface brightness.[6] Although the scatter measured by chi-square does not decrease (in fact increases slightly), the slope of the relation flattens, and a given uncertainty in velocity width translates to a smaller uncertainty in magnitude. Figure 5 displays the results graphically. The resulting scatter is, however, still too large to be explained entirely by the depth of the cluster. Since a variety of other galaxy parameters might have been (and were) tested for their ability to reduce the dispersion, the usefulness of this one must be verified on an independent sample before being accepted.

5. CHANGING THE SAMPLE

Having found which input data give a Tully-Fisher relation with the least scatter, we here investigate whether changing the sample can affect the conclusions. Table 7 and Figure 6 show the results for the complete sample given in Table 1. The principal result is that even after consideration of the known uncertainties in the observations, there remains uncertainty in the magnitude of an individual galaxy of 0.36 mag once the effect of the expected cluster depth (0.17 mag) is removed. This is in agreement with the value found for Virgo in Paper I.

5.1. *Previous Work*

PT obtained CCD images in B, R, and I for 26 Ursa Major galaxies and obtained total magnitudes in these bands. For 18 of these, $H^c_{-0.5}$ magnitudes had been obtained by A82. PT found a scatter around the Tully-Fisher relation of ~0.30 mag in R, I, and H. Corrected for uncertainties in the observations, they needed an intrinsic scatter of only 0.22 mag, which is statistically consistent with the depth of the cluster (~0.17 mag if the cluster is a sphere). However, the sample by PT is not complete, although for $B_T < 13.3$ mag it contains most cluster members.[7]

[6] The uncertainties in central surface brightness are not important, since this is a second-order correction, so only uncertainties in magnitudes and velocity widths have been considered. The fit chosen was the one that minimizes the additional magnitude uncertainty needed to give a reduced chi-square of one, not the one that minimizes chi-square itself. The fit is rather insensitive to the exact coefficient of the $H(0)$ term with values between 0.2 and 0.5 giving about the same result.

[7] The PT sample contains five galaxies that we rejected from our initial sample (Table 2) and one more (UGC 6816) that is 8° from our adopted cluster center. However, of these rejected galaxies, only NGC 3782 has H band photometry. Thus the main difference between our samples is that we have added eight galaxies (plus NGC 4218 which we did not observe) not included by PT. As noted, we have also measured two galaxies that were included in their sample but had no H photometry.

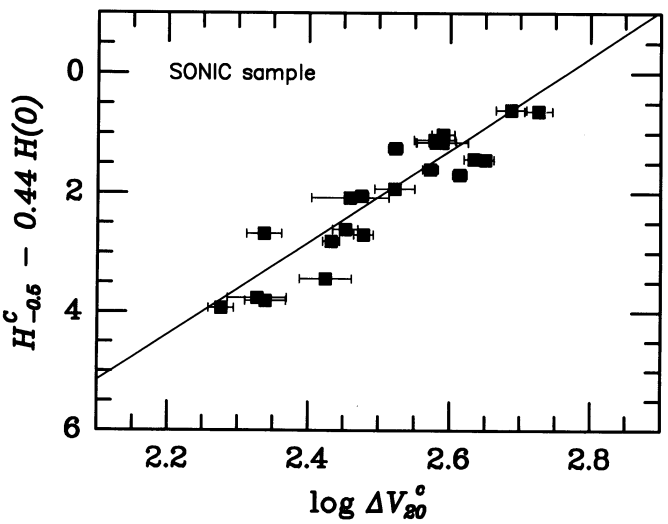

FIG. 5.—Tully-Fisher diagram with a third parameter. Adjusting the magnitude by the central surface brightness of the disk gives a flatter slope and less dispersion in the magnitude axis. The line shows the best-fit relation from Table 6.

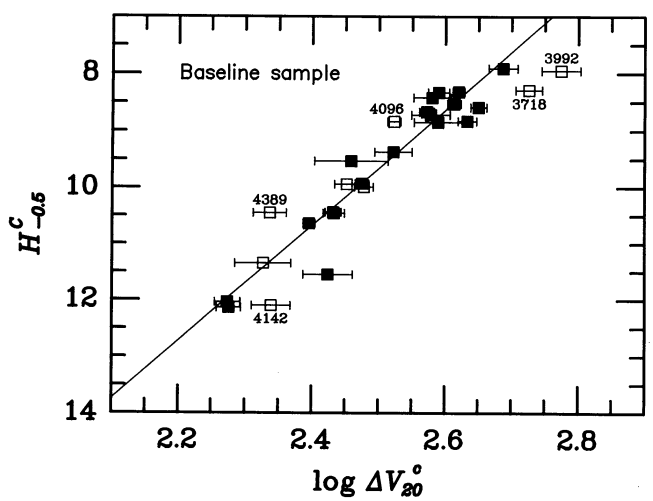

FIG. 6.—Tully-Fisher diagram for the baseline sample. Galaxies previously observed by PT are shown with filled symbols while those added are shown by open symbols. Vertical error bars are not shown because they are almost all smaller than the symbols. The line shows the best-fit relation from Table 7. NGC numbers are shown for five of the galaxies with the largest deviations.

TABLE 7

LEAST-SQUARE FIT RESULTS—CHANGING SAMPLE

Velocity Widths (1)	Nonrotational Correction (2)	Inclination Source (3)	Sample (4)	N_{gal} (5)	χ^2_{red} (6)	Δ(mag) (7)	Slope (8)	Intercept (9)
Baseline								
RC3	no	RC3	Table 1	27	4.32	0.40	0.098	2.564
Comparison with PT								
PT	yes	PT	PT	18	2.84	0.20	0.106	2.516
PT	yes	PT	PT + 2	20	2.64	0.20	0.106	2.516
RC3	yes	PT	PT + 2	20	2.78	0.20	0.109	2.513
RC3	no	PT	PT + 2	20	2.54	0.19	0.095	2.563
RC3	no	RC3	PT + 2	20	2.59	0.26	0.097	2.566
RC3	no	RC3	omit 3782	19	2.50	0.24	0.096	2.566
Omit NGC 3718								
RC3	no	RC3	Table 1	26	3.99	0.38	0.096	2.562
Omit NGC 4389								
RC3	no	RC3	Table 1	26	4.00	0.37	0.096	2.565
Omit NGC 3718 and NGC 4389								
RC3	no	RC3	Table 1	25	3.65	0.34	0.094	2.563
Omit NGC 4096								
RC3	no	RC3	Table 1	26	3.58	0.38	0.099	2.570
Bright galaxies: log $\Delta V^c > 2.43$								
RC3	no	RC3	Table 1	20	4.44	0.31	0.104	2.565
Galaxies with $600 < V_H < 1025$ km s^{-1}								
RC3	no	RC3	Table 1	18	2.20	0.26	0.095	2.557
Galaxies with $600 < V_H < 985$ km s^{-1}								
RC3	no	RC3	Table 1	17	1.32	0.12	0.092	2.553

NOTES.—(col. [1]) Source of velocity widths; (col. [2]) correction for non-rotational motion (W_R); (col. [3]) source of inclinations; (col. [4]) sample; (col. [5]) number of galaxies in sample; (col. [6]) reduced χ^2 of fit; (col. [7]) additional uncertainty in the H-magnitudes necessary to bring χ^2 down to unity; (cols [8] and [9]) best slope a and intercept b for $\log \Delta V = -a(H - 9.0) + b$. For the baseline, the uncertainty in the slope is 0.006, and the uncertainty in the intercept is 0.008.

As in Paper I, we have reanalyzed their sample with new velocity widths and magnitudes. Table 7 compares Tully-Fisher fits for our sample and for the PT sample. The first line of the PT results uses only their data except that the older magnitudes have been replaced by ours. Successive lines show the effect of including the two galaxies not previously measured, using RC3 velocity widths, removing the velocity width correction for nonrotational motions, and using inclinations derived from the RC3 instead of the PT inclinations. None of these changes makes any difference in the scatter as measured by χ^2, although the last one does increase the inferred magnitude uncertainty.[8] Figure 7 shows the Tully-Fisher relation derived from both sets of inclinations. Almost all of the increased magnitude uncertainty comes from UGC 6983, to which PT assign an inclination of 55° while the RC3 axis ratios imply $i \approx 47°$. Nevertheless, for this sample, for all choices of velocity widths, correction procedures, and inclinations, the intrinsic scatter after correcting for observational uncertainties is not much more than 0.2 mag, in agreement with that found by PT. The additional scatter found in our complete sample must therefore be contributed by the galaxies not included in the PT sample. This increased scatter is inconsistent with the expected cluster depth and may be regarded as intrinsic scatter in the magnitude of an individual galaxy. Some possible causes of the scatter were discussed in Paper I.

[8] Table 7 also shows that omitting NGC 3782, the only galaxy in the PT sample but not in ours, makes little difference.

5.2. *Outlier Galaxies*

As shown in Figures 6, the two galaxies with the largest residuals are among the eight absent from the PT sample. Six of the eight galaxies have residuals larger than the 1 σ values, as opposed to 3 one would expect from Gaussian statistics. The four galaxies causing most of the extra scatter are the two bright galaxies, NGC 4389, and possibly UGC 6894. It is debatable that PT did not include NGC 3718, since in the RC3 it has been classified as peculiar or a merger remnant, but there is no obvious reason why the brightest cluster member, NGC 3992, was not included.

NGC 3718 has a regular H I profile and does not look disturbed in the H band. However, in the optical a prominent

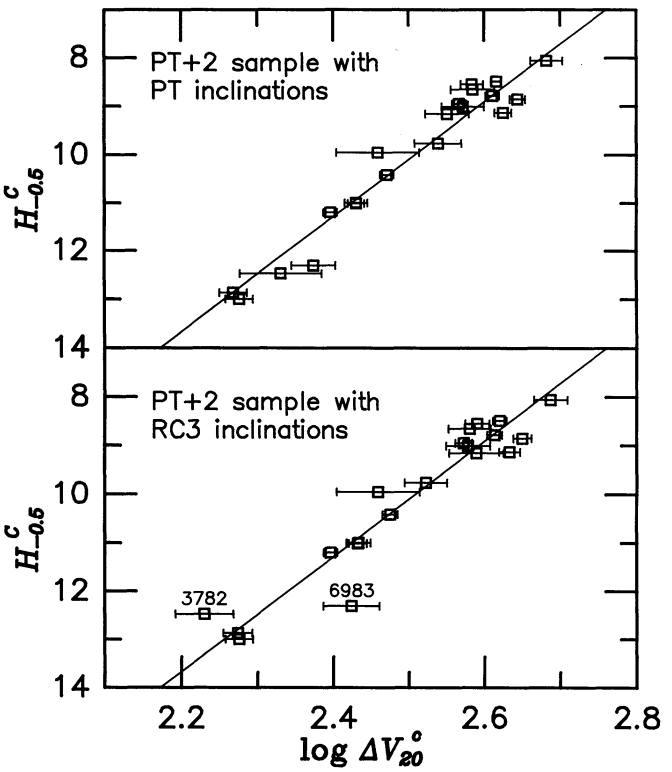

FIG. 7.—Tully-Fisher diagram for the PT sample of galaxies in the Ursa Major cluster. Part (*a*) uses inclinations from PT, part (*b*) from the RC3.

dustlane is visible, together with faint structure in the outer regions. The gas distribution can be explained well by a warped disk with a tilt of almost 90° (Schwarz 1985). Given this extra information that the dynamics of this galaxy are dissimilar to a rotating disk, one is justified in removing it from the sample. However, if only the minimum information required to use this galaxy in the Tully-Fisher relation were available, as is usually the case, one would have no reason to reject it. Changing the inferred inclination of the galaxy would not bring it closer to the Tully-Fisher relation. The optical axis ratio from the RC3 was taken in the outer regions, where the galaxy is the most elongated, so that the inclination correction is minimized. An inclination derived from photometry in the inner parts (e.g., the *H*-photometry) would only increase the deviation. If we reject NGC 3718 from the sample we see that the scatter decreases only slightly (Table 7).

Inclusion of NGC 3718 and 3992 makes it appear that the Tully-Fisher relation levels off at large velocity width, i.e., that above a velocity width of $\sim$450 km s^{-1} galaxies have a constant brightness rather than a further increase. The turnover[9] is also seen in the data presented by AHM (Fig. 2), PT (Fig. 3), and Giraud (1986, Fig. 5), although these authors did not comment on it. No turnover is seen, however, in observations of the Coma cluster (S. Raychaudhury 1993, private communication).

[9] To avoid confusion, we use the word "turnover" for possible leveling off at the bright end of the Tully-Fisher relation. It should not be confused with "curvature" at the faint end. The latter can always be eliminated by a suitable choice of correction for nonrotational velocities.

The deviation of NGC 4389 might be caused by an underestimated velocity width. Contrary to most of the other galaxies in his sample, the velocity profile of NGC 4389 is not symmetric (Huchtmeier 1982). Its type, Sa, is another indication that this galaxy might be deficient in H I. Table 7 shows the effect on the Tully-Fisher relation of omitting NGC 4389. The scatter goes down, but the remainder is still too large to be caused by cluster depth. Even omission of both NGC 3718 and 4389 does not reduce the scatter to the level found by PT.

We have also considered the possibility that for the faintest galaxies, the systematic errors are much larger than assumed. Since even in *B*, surface brightness decreases as a function of velocity width, the circular magnitudes might not be adequate any more; systematic errors in the bulge-disk decomposition might equally well affect the total magnitudes. Table 7 shows results for a sample of galaxies with log $\Delta V^c > 2.43$. The residuals from the Tully-Fisher relation here are smaller than for the complete sample but still closer to 0.4 than to 0.2 mag. The scatter remaining is caused by the turnover at the bright end of the relation.

Excluding NGC 4096, the one galaxy in our sample correctly assigned to group 14-4 instead of 12-1 (NBG), makes no significant difference in the results.

5.3. *Evidence of Subclustering*

Although our definition of "the Ursa Major Cluster" has closely followed previous work, one interpretation of our data is that there is a background subcluster superposed on the main cluster. Figure 8 shows the residuals from the Tully-Fisher relation plotted as a function of heliocentric radial velocity. The four galaxies with large residuals (in the sense that they are fainter than expected for their velocity widths) all have radial velocities $\gtrsim$1000 km s^{-1}. Galaxies with high velocity (including rejected galaxies) are mostly located north of the cluster center, though some are found to the south as well. The data of PT show no evidence for a background subcluster, nor are we aware of any previous suggestion of one, but the possibility must be mentioned.

If galaxies with radial velocity greater than 1025 km s^{-1} (or less than 600 km s^{-1}) are excluded from the sample, the derived intrinsic scatter drops to 0.26 mag (Table 7). This

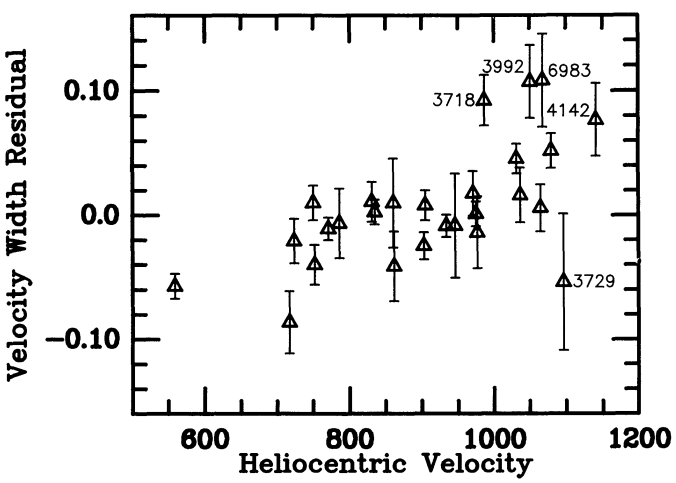

FIG. 8.—Residuals from the Tully-Fisher relation as a function of heliocentric radial velocity. Galaxies having large residuals are identified with NGC or UGC numbers. A positive residual implies that the galaxy is too faint for its velocity width.

approaches the amount of scatter from the expected cluster depth. If the upper cutoff is reduced to 985 km s^{-1} so as to exclude NGC 3718, the intrinsic scatter drops to 0.12 mag, significantly less than expected.

6. DISCUSSION

6.1. *Intrinsic Scatter*

In the previous section it was found that for a complete sample in Ursa Major, selected in ΔV^c, the scatter in the Tully-Fisher relation is larger than can be explained by known observational uncertainties or the depth of the cluster, assuming it is spherical. Since PT obtained a dispersion that was consistent with no intrinsic scatter, and our samples differ basically in the brightest and faintest galaxies, it is possible that the scatter originates from curvature in the relation rather than from intrinsic scatter at each velocity width. Even when removing the faint galaxies ($\Delta V \leq 2.43$), for which the observational uncertainties might be larger than estimated, the scatter remains 0.31 mag after correcting for observational uncertainties. A turnover at the bright end of the Tully-Fisher relation in Ursa Major is a possible explanation. Curvature at the faint end of the Tully-Fisher relation was discussed earlier by A82, Aaronson & Mould (1983), Bottinelli et al. (1984), and others. Bottinelli et al. pointed out that this could be an artifact of the line width definition, and PT found no curvature when using W_R instead of ΔV^c_{20}. However, Table 5 shows that correcting for nonrotational motion has no significant effect on the scatter.

Two recent studies of the *I*-band Tully-Fisher relation (Mathewson, Ford, & Buchhorn 1992; Schommer et al. 1993) obtained values for the scatter that are much lower than we find for Ursa Major.[10] However, neither of these studies claim to be complete in any sense, and Schommer et al. observed very few cluster members. If more detailed study shows such low scatter to be real, the substructure in Ursa Major must be taken seriously.

In this paper we found an enormous amount of curvature when using magnitudes defined using infrared isophotes. Since the disk surface brightness decreases rapidly as a function of ΔV (Table 4), the ratio between isophotal and total magnitude changes with it in a nonlinear way. In *B* when the diameter used for $H^c_{-0.5}$ is determined, the central surface brightness is roughly constant for bright galaxies but decreases with luminosity for faint galaxies (e.g., Peletier & Willner 1992). Since the latter effect is much weaker than in *H*, the use of $H^c_{-0.5}$ might result in some subtle curvature. This cannot be the cause of the observed scatter, however, because the scatter remains even if faint galaxies are excluded or if velocity widths are corrected for nonrotational motions.

The turnover at large ΔV remains if we use total magnitudes but can be removed by taking the central surface brightness of the disk, $H(0)$, as a third parameter (Fig. 5). Even with this third parameter, the magnitude dispersion is still too large to be explained by the observations alone. The dependence of magnitude on ΔV and $H(0)$ may be nonlinear, not only the ΔV-dependence (the curvature), but also the $H(0)$-dependence. Bothun & Mould (1987) suggested that by using the surface brightness profiles (not just central surface brightness), they could decrease the scatter in the Tully-Fisher relation. If nonlinear relations are allowed, many more galaxies must be observed to determine the additional free parameters. In any case, there seems no way of avoiding significant intrinsic scatter in the conventional *linear* Tully-Fisher relation.

[10] Schommer et al. (1993) found a scatter of 0.29 mag for Hydra and only 0.18 mag for Antlia. Matthewson et al. (1992) found 0.25 mag for Fornax. These values appear to represent the *total* scatter, i.e., to include the scatter due to observational uncertainties.

6.2. *The Slope of the Tully-Fisher Relation*

Depending on the choice of magnitude and sample, most of the slopes we find lie between 0.09 and 0.11 (for $\log \Delta V^c = -aH + b$), corresponding to a conventional slope ($H = -a' \log \Delta V^c + b'$) between 9 and 11. This is consistent with Virgo cluster (Paper I), although that sample was magnitude-selected and therefore potentially biased in slope. PT show that for *B*, *R*, and *I* the slope using total magnitudes is smaller than when using aperture magnitudes. We find the same in *H* (10.2 ± 0.6 vs. 9.3 ± 1.0) for $H^c_{-0.5}$ and H_T for our largest possible samples. However, the slope for total magnitudes is not 8, as PT predict, but close to 10, a value that is expected for $\Delta V^c \propto M^4$ (as expected if the central mass surface density of galaxies is constant) and a constant M/L (AHM79). Since the total magnitudes in this paper have all been determined using extrapolation, this conclusion will have to be tested with deeper surface photometry.

6.3. *Difference between Ursa Major and Virgo*

Although we find significantly larger scatter in both clusters than did PT, we confirm their result that the scatter in Ursa Major is smaller than in Virgo. From this it follows that there must be some substructure in Virgo or that the Virgo cluster is elongated toward us, or the Tully-Fisher intrinsic scatter varies from cluster to cluster. Our zero points for Virgo and Ursa Major are almost identical (for the "baseline" 2.547 in Virgo and 2.564 in Ursa Major), so it appears that the center of Virgo is $8 \pm 3\%$ closer than Ursa Major, in agreement with PT. However, this conclusion should be regarded with caution, since the Virgo sample was magnitude selected and therefore potentially biased in magnitude.

6.4. *Extinction in H*

Even in *H*, galaxies might still contain reasonable amounts of extinction (Peletier & Willner 1992). A typical face-on extinction of 0.07 magnitudes corresponds to 0.20 mag for a galaxy with inclination 70°, typical of this sample. Bothun & Mould (1987) derived a typical reddening-correction to their *I* data of 0.30 mag. Using the galactic extinction law (Schultz & Wiemer 1975) this corresponds to 0.11 mag in *H*. Either amount would be enough to cause measurable scatter in the Tully-Fisher relation. We have found no correlation between inclination and total *H*-magnitude, but our sample is small, and our total magnitudes are uncertain. There is also no correlation between inclination and residual other than the expected greater scatter for lower inclinations. Since the reddening is very uncertain, a study of the infrared color profiles of spiral galaxies is important to determine whether absorption causes any of the scatter in the Tully-Fisher relation, even in *H*.

Freeman's (1970) law, which states that the central surface brightness of disks of spiral galaxies of types Sa-Sc is constant at $B = 21.6$ mag arcsec^{-2} with a scatter of only 0.3 mag, implies that the centers of some disks are very red in $B-H$. Some galaxies have central disk colors of $B-H = 6.0$ mag. Since a typical elliptical galaxy (thus presumably a typical spiral bulge) has a $B-H \approx 3.9$, there has to be at least 2.5 mag

of extinction in B or possibly more, depending on the geometry. Many galaxies of this sample are so red in the center that they are optically thick in B. The colors will be discussed further elsewhere.

7. CONCLUSIONS

From a H band imaging study of a complete sample of galaxies in the Ursa Major cluster, selected on the basis of velocity width we conclude:

1. The scatter in the Tully-Fisher relation is least when using circular magnitudes within an optically determined diameter. Infrared isophotal magnitudes give very bad fits owing to the strong relation between velocity width and surface brightness. Using extrapolated total magnitudes the scatter is worse than using circular magnitudes. It is still possible, however, that total magnitudes measured from deeper images may match or improve upon circular magnitudes.

2. The scatter in the Tully-Fisher relation in Ursa Major is larger than can be accounted for by its depth. After taking into account uncertainties in the observations and a cluster depth of 0.17 mag, an intrinsic scatter in the magnitude of an individual galaxy of order 0.36 mag is needed.

3. The scatter in the Ursa Major cluster is slightly smaller than in Virgo. This is evidence for subclustering in Virgo, assuming that both clusters are spherical.

4. The slope of the Tully-Fisher relation in total H-magnitudes is 10.2 ± 0.6 (for $H^c_{-0.5}$ magnitudes and ΔV^c_{20} velocity widths). Since the stellar M/L in this band is rather insensitive to metallicity, this slope corresponds to $M \propto V^{4.1 \pm 0.3}$, in agreement with AHM but not with PT.

5. Dust absorption might cause scatter of ~ 0.1 mag, but we see no direct evidence for it.

6. The Tully-Fisher relation in Ursa Major appears to turn over at large velocity widths.

7. Distance estimates may be slightly improved if the central surface brightness of the galaxy disk is added as a third parameter. This means that the Tully-Fisher relation can better be replaced by a magnitude–velocity width–surface brightness plane. The usefulness of this relation be tested on an independent sample.

8. There is evidence for a background subcluster superposed on the northern part of the Ursa Major cluster at a heliocentric velocity $\gtrsim 1000$ km s^{-1} If this subcluster is real, the intrinsic scatter in the Tully-Fisher relation might be quite small.

We thank J. Huchra for permission to use the redshift survey data and C. Clemens and E. Falco for facilitating our access. We thank M. Franx for providing the GALPHOT program, for stimulating discussions about spiral galaxies, and for valuable comments on the manuscript. We are indebted to S. Raychaudhury for raking some of the images for this project and for showing us his Coma data prior to publication. J. Geary, W. Wyatt, and C. Hughes constructed major parts of SONIC. We thank D. Mink for help with the software and B. van't Sant and T. Groner for help at the telescope. Part of this work was done during a visit of R. F. P. at the CfA supported by the Smithsonian Short-Term Visitor Program. This research was partially supported by grants from the Scholarly Studies Fund of the Smithsonian Institution and was greatly facilitated by use of the NASA/IPAC Extragalactic Database (NED) which is operated by the Jet Propulsion Laboratory, California Institute of Technology, under contract with the National Aeronautics and Space Administration.

REFERENCES

Aaronson, M., Bothun, G., Mould, J., Huchra, J., Schommer, R. A., & Cornell, M. E. 1986, ApJ, 302, 536
Aaronson, M., Huchra, J., & Mould, J. 1979, ApJ, 229, 1 (AHM)
Aaronson, M., & Mould, J. 1983, ApJ, 265, 1
Aaronson, M., Mould, J., & Huchra, J. 1980, ApJ, 237, 655 (AMH)
Aaronson, M., et al. 1982, ApJS, 50, 241 (A82)
Biviano, A., Giuricin, G., Mandirossian, F., & Mezzetti, M. 1990, ApJS, 74, 325
Bothun, G. D., & Mould, J. R. 1987, ApJ, 313, 629
Bothun, G. D., Mould, J., Schommer, R. A., & Aaronson, M. 1985, ApJ, 291, 586
Bottinelli, L., Fouqué, P., Gouguenheim, L., Paturel, G., & Teerikorpi, P. 1987, A&A, 181, 1
Bottinelli, L., Gouguenheim, L., Fouqué, P., & Paturel, G. 1990, A&AS, 82, 391
Bottinelli, L., Gouguenheim, L., Paturel, G., & de Vaucouleurs, G. 1983, A&A, 118, 4
———. 1984, ApJ, 280, 34
Bottinelli, L., Gouguenheim, L., Paturel, G., & Teerikorpi, P. 1988, ApJ, 328, 4
de Vaucouleurs, G., de Vaucouleurs, A., & Corwin, H. G., Jr. 1976, Second Reference Catalog of Bright Galaxies (Austin: Univ. Texas Press) (RC2)
de Vaucouleurs, G., de Vaucouleurs, A., Corwin, H. G., Jr., Buta, R. J., Paturel, G., & Fouqué, P. 1991, Third Reference Catalog of Bright Galaxies (NY: Springer) (RC3)
Elias, J. H., Frogel, J. A., Matthews, K., & Neugebauer, G. 1982, AJ, 87, 1029
Fouqué, P., Bottinelli, L., Gouguenheim, L., & Paturel, G. 1990, ApJ, 349, 1
Franx, M., & de Zeeuw, P. T. 1992, ApJ, 392, L47
Freedman, W. L. 1990, ApJ, 355, L35
Freeman, K. C. 1970, ApJ, 160, 811
Geller, M. J., & Huchra, J. P. 1983, ApJS, 52, 61
Giraud, E. 1986, ApJ, 301, 7
Helou, G., Hoffman, G. L., & Salpeter, E. E. 1984, ApJS, 55, 433
Huchra, J., Davis, M., Latham, D., & Tonry, J. 1983, ApJS, 52, 89
Huchra, J. P., & Geller, M. J. 1982, ApJ, 257, 423
Huchtmeier, W. K. 1982, A&A, 110, 121
Jacoby, G. H., et al. 1992, PASP, 104, 599
Jørgensen, I., Franx, M., & Kjærgaard, P. 1992, A&AS, 95, 489
Kent, S. M. 1986, AJ, 91, 1301
Kraan-Korteweg, R. C., Cameron, L. M., & Tammann, G. A. 1988, ApJ, 331, 620
Mathewson, D. S., Ford, V. L., & Buchhorn, M. 1992, ApJ, 389, L5
Peletier, R. F., & Willner, S. P. 1991, ApJ, 382, 382 (Paper I)
———. 1992, AJ, 103, 1761
Pierce, M. J., & Tully, R. B. 1988, ApJ, 330, 579 (PT)
Schommer, R. A., Bothun, G. D., Williams, T. B., & Mould, J. R. 1993, AJ, 105, 97
Schultz, G. V., & Wiemer, W. 1975, A&A, 43, 133
Schwarz, U. J. 1985, A&A, 142, 273
Teerikorpi, P. 1984, A&A, 141, 407
———. 1987, A&A, 173, 39
Tully, R. B. 1987, ApJ, 321, 280
———. 1988, Nearby Galaxies Catalog (Cambridge: Cambridge Univ. Press) (NBG)
Tully, R. B., & Fisher, J. R. 1977, A&A, 54, 661
Tully, R. B., & Fouqué, P. 1985, ApJS, 58, 67
Turner, E. L., & Gott, J. R. 1976, ApJS, 32, 409